Electronic Supplementary Information

Engineering FeCo alloy@N-doped carbon layers by directly pyrolyzing Prussian blue analogue: new peroxidase mimetic for chemiluminescence glucose biosensing

Yuwan Lu, Xiaodan Zhang, Xuanxiang Mao, Yuming Huang*

The Key Laboratory of Luminescence and Real-Time Analytical Chemistry, Ministry of Education, College of Chemistry and Chemical Engineering, Southwest University, Chongqing 400715, China.

Corresponding author. E-mail: ymhuang@swu.edu.cn

General procedure for CL detection

Fig. S1 shows a diagram of the flow injection CL detection system, Two peristaltic pumps were used to deliver the solutions, in which one delivers FeCo@NC suspension and water carrier stream, the other does luminol solution and H_2O_2 (or sample solution). The produced CL signal was monitored by a PMT (at a working voltage of –600 V) and recorded by a computer. The data was processed by REMAX software. The net CL intensity ($\Delta I=I-I_0$, where I and I_0 were the CL intensity of sample and blank solutions, respectively) versus the concentration of target was used for calibration. At each target concentration, the injection was repeated for at least three times, and the average CL signal was recorded.

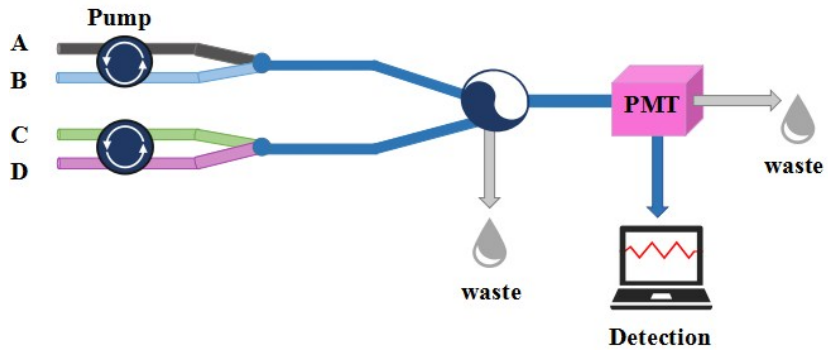

Fig. S1. Schematic diagram of the FIA (flow injection analysis)–CL system. A: FeCo@NC suspension; B: water carrier stream; C: luminol solution; D: H_2O_2 or sample solution; PMT: photomultiplier tube, PC: personal computer.

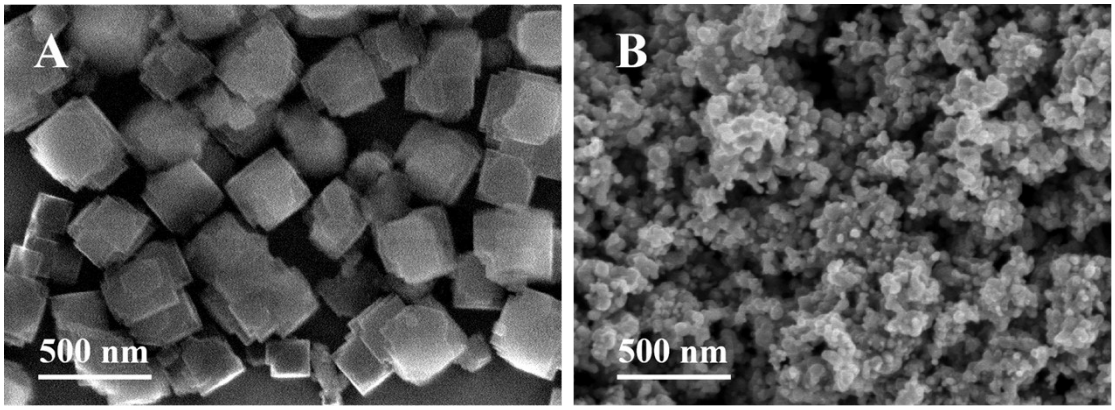

Fig. S2. SEM images of (A) Fe^{III}-Co PBA and (B) FeCo@NC-600.

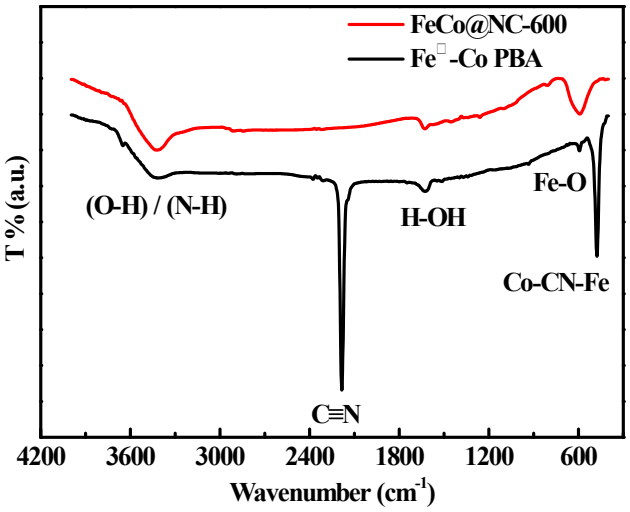

Fig. S3. FT-IR spectra of Fe^{III}-Co PBA and FeCo@NC-600.

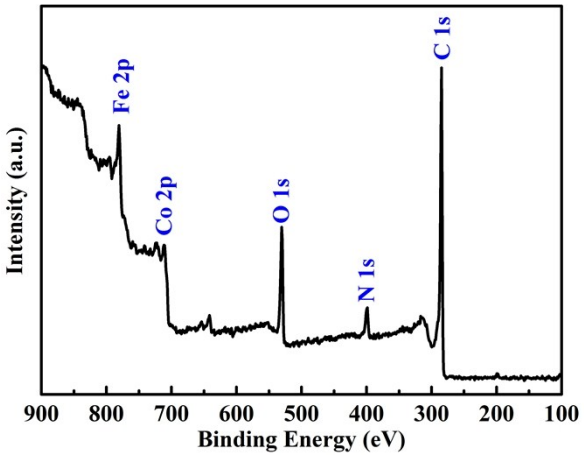

Fig. S4. XPS survey spectra for FeCo@NC-600.

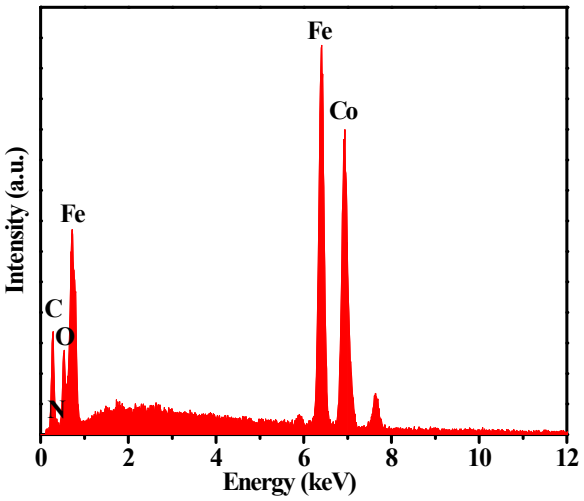

Fig. S5. EDS spectrum of FeCo@NC-600.

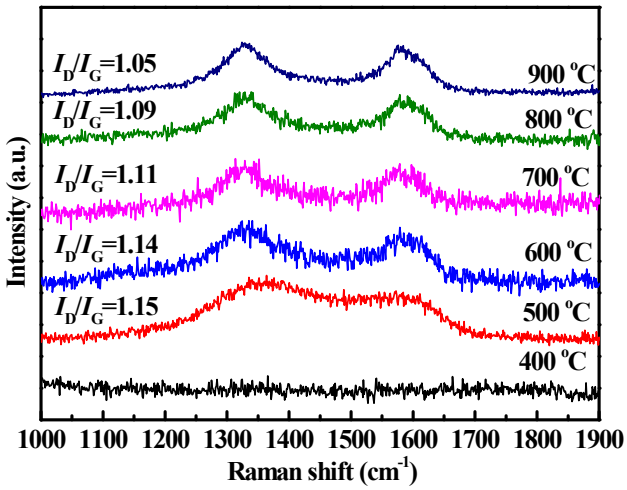

Fig. S6. Ramen spectrum of the FeCo@NC-X obtained at different carbonization temperature in the 400 °C to 900 °C range.

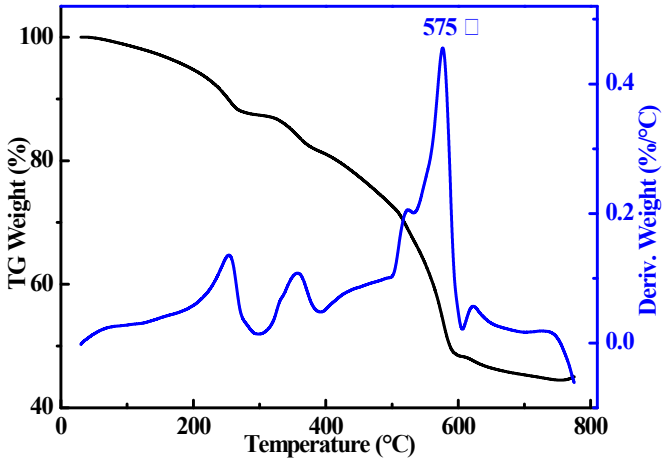

Fig. S7. TG-DTG curves of Fe^{III}-Co PBA in N_2 atmosphere.

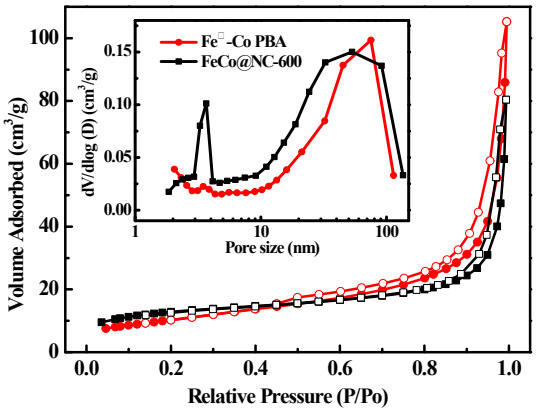

Fig. S8. N_2 adsorption-desorption isotherms of Fe^{III}-Co PBA and FeCo@NC-600. Inset: Pore size distribution curves of Fe^{III}-Co PBA and FeCo@NC-600.

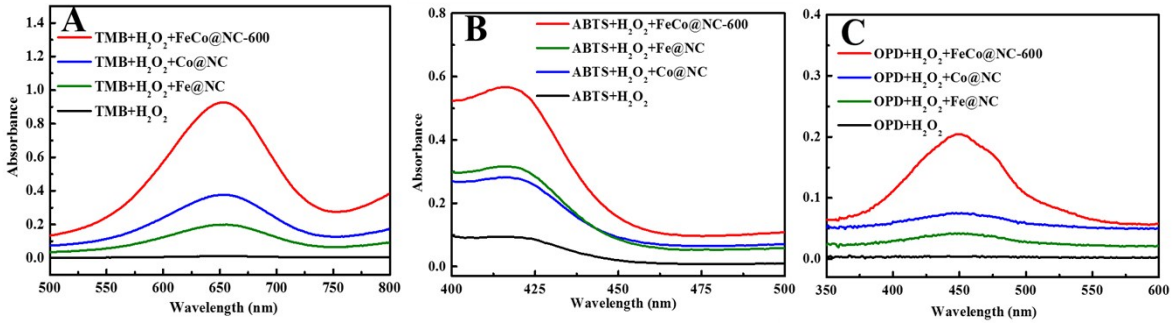

Fig. S9. The UV-visible absorption spectra of (A) TMB–H_2O_2, (B) ABTS–H_2O_2 and (C) OPD–H_2O_2 systems in the presence of different catalysts. Reaction conditions: Concentration of TMB, ABTS and OPD: 0.5 mM; 0.1 mM H_2O_2; Concentration of FeCo@NC-600, Fe@NC and Co@NC): 10 mg/L; pH 3.5 (0.2 M HAc-NaAc); 20 min reaction at room temperature.

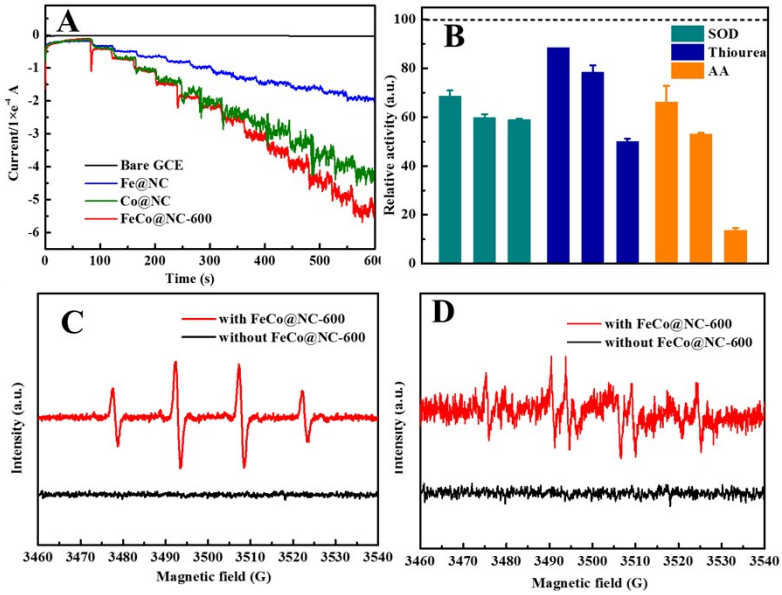

Fig. S10. (A) Amperometric response of bare GCE (glassy carbon electrodes), Fe@NC modified GCE, Co@NC modified GCE and FeCo@NC-600 modified GCE in 0.1 M PBS buffer (pH 7.4) at applied potential of -0.4 V upon successive addition of 1.0 M H_2O_2 at time intervals of 40 s. (B) The relative activity of FeCo@NC-600 with different radical scavengers. SOD concentration: 50 U/mL; 100 U/mL and 200 U/mL; AA concentration: 0.04 mM; 0.1 mM and 0.2 mM; Thiourea concentration: 0.5 mM; 1 mM and 2.5 mM. (C) ESR spectra of •OH radicals in the H_2O_2-DMSO system with and without FeCo@NC-600. (D) ESR spectra of $\bullet O_2^-$ radicals in the H_2O_2-DMPO system with and without FeCo@NC-600.

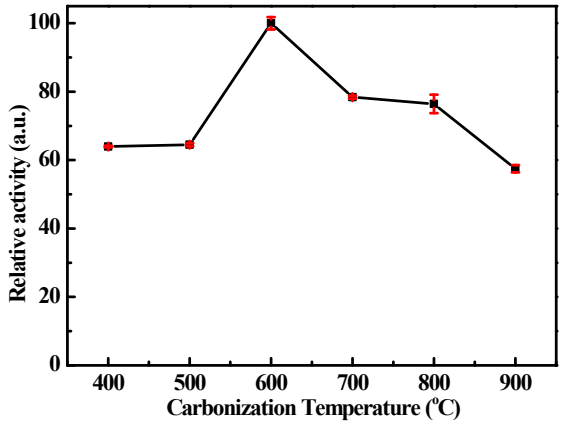

Fig. S11. Effect of carbonization temperature on the activity of the resultant FeCo@NC-X.

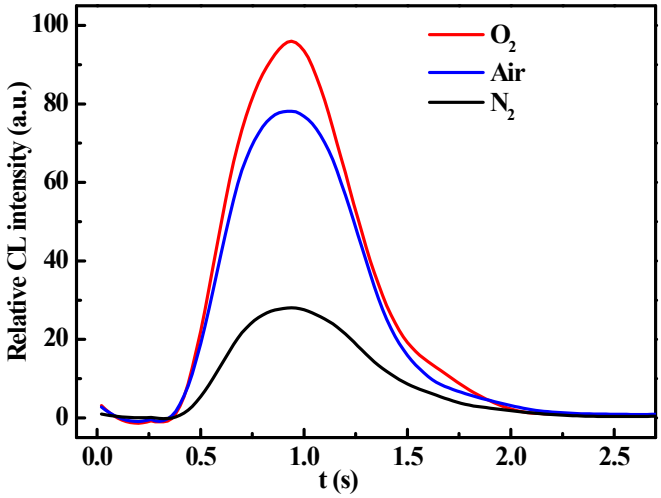

Fig. S12. CL kinetic curves of luminol-H_2O_2-FeCo@NC-600 system in O_2-saturated (red), air-saturated (blue) and N_2-saturated solutions (black), respectively.

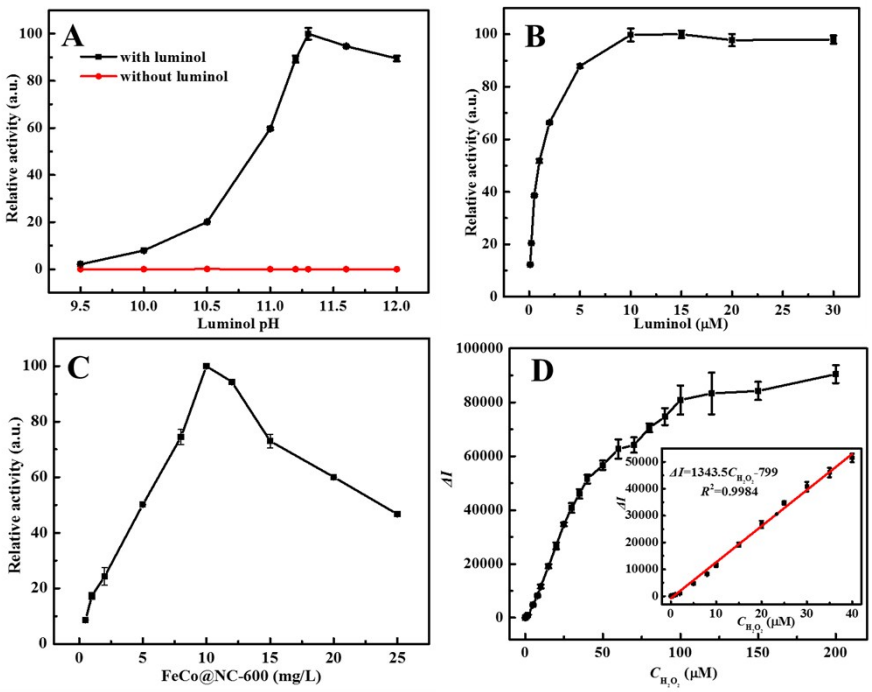

Fig. S13. (A) Effect of pH of luminol: 10 μM luminol, 0.5 μM H_2O_2, 10 mg L^{-1} FeCo@NC-600. (B) Effect of luminol concentration: 0.1 M Na_2CO_3-$NaHCO_3$ buffer solution (pH 11.3), 0.5 μM H_2O_2, 10 mg L^{-1} FeCo@NC-600. (C) Effect of FeCo@NC-600 concentration: 10 μM luminol in 0.1 M Na_2CO_3-$NaHCO_3$ buffer solution (pH 11.3), 1.0 μM H_2O_2. Error bars represent the standard deviation for three replicates detection. (D) The response curve of H_2O_2 under the optimized conditions. Inset: the linear relationship between net CL intensity and concentration of H_2O_2. Error bars were acquired from three replicates determination.

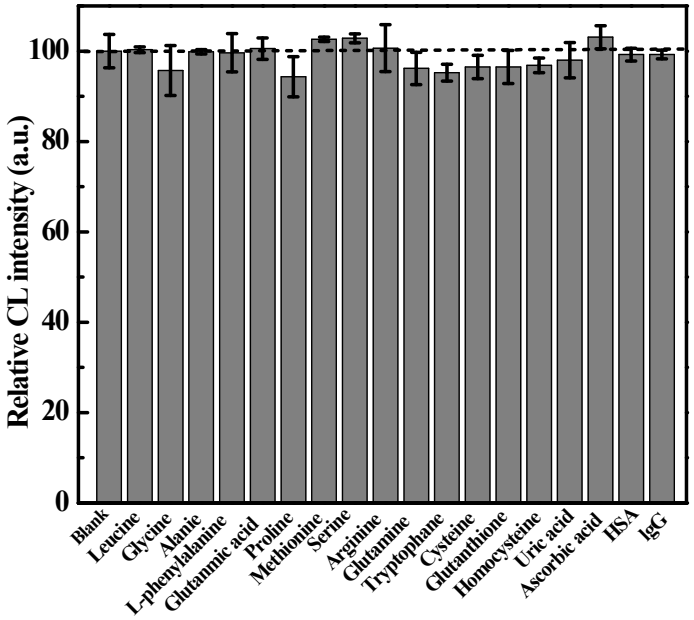

Fig. S14. Selectivity of the proposed method for H_2O_2 detection in the present of potential interfering substances. Blank: 1 μM H_2O_2. The concentrations of tested substances were 1 mM for leucine, glycine, alanie, L-phenylalanine and glutanmic acid, 0.5 mM for proline, methionine, serine, arginine and glutamine, 10 μM for tryptophane, 5 μM for cysteine, glutanthione and homocysteine, 1 μM for uric acid and ascorbic acid, 100 mg/L for HSA (human serum albumin) and 10 mg/L for IgG (immunoglobulin G), respectively. The error bars represents standard deviations based on three independent measurements.

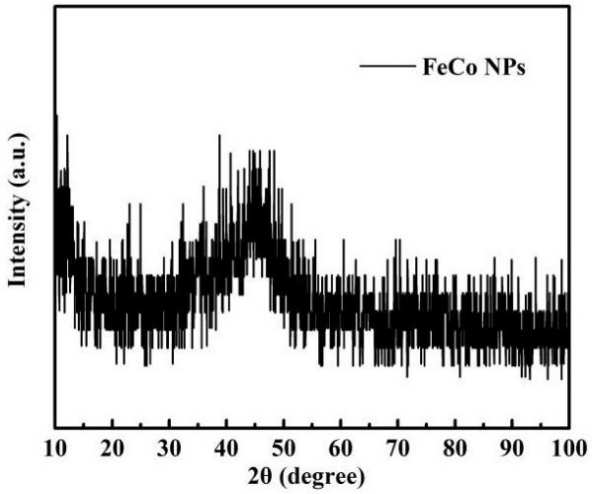

Fig. S15. XRD spectra of the synthesized FeCo NPs.

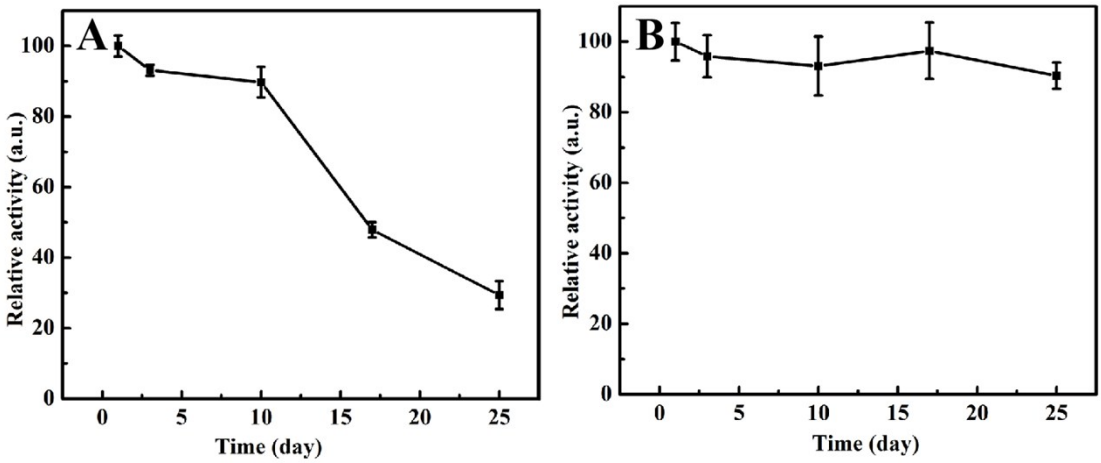

Fig. S16. Variation of catalytic activity of the (A) FeCo NPs and (B) FeCo@NC-600 with storage time.

Table S1. Atomic concentration (%) of C, N, O, Fe, and Co in FeCo@NC-600.

Element	*At % from EDS*	*At % from XPS*
C	36.41	71.87
N	2.61	7.89
O	5.99	12.38
Fe	29.15	4.49
Co	25.84	3.37

Table S2. The surface area and pore volume of Fe^{III}-Co PBA and FeCo@NC-600.

Samples	Surface area (m^2/g)	Total pore volume (cm^3/g)
Fe^{III}-Co PBA	42.84	0.12
FeCo@NC-600	37.63	0.16

Table S3. Atomic concentration (%) of N in FeCo@NC-X.

Samples	At % of N
FeCo@NC-500	11.7
FeCo@NC-600	7.89
FeCo@NC-700	6.66
FeCo@NC-800	2.82
FeCo@NC-900	1.93

Table S4. Recoveries of 1 μM H_2O_2 in the presence of foreign species.

Coexisting species	Concentration (mg/L)	Recovery (%)	Coexisting species	Concentration (mg/L)	Recovery (%)
Na^+	23	101.90±2.19	Al^{3+}	1.08	99.60±1.30
K^+	31.2	100.00±3.23	Cl^-	35.5	101.90±2.19
NH_4^+	7.2	103.25±0.11	Br^-	1.6	100.14±0.72
Ca^{2+}	16	105.38±0.57	NO_3^-	24.8	96.71±0.38
Mg^{2+}	4.8	96.71±0.38	SO_4^{2-}	48	103.29±3.08
Zn^{2+}	0.33	99.18±2.04	NO_2^-	0.46	102.19±0.61
Pb^{2+}	4.1	102.52±1.84	SO_3^{2-}	0.8	94.21±0.80
Ni^{2+}	0.3	8.67±1.73	HPO_4^{2-}	1.92	100.01±2.05
Cr^{3+}	52*	98.31±1.13	$H_2PO_4^-$	9.7	103.92±2.36
Ba^{2+}	1.37	95.84±1.65	PO_4^{3-}	0.48	99.80±0.43

* μg L^{-1}

Table S5. Comparison of the linear ranges and detection limits for glucose afforded by the proposed and other CL methods.

System	Linear range (M)	LOD (M)	Refs
ECL-GOD/AuNPs/PANi	1.0×10^{-7}-1.0×10^{-4}	5.0×10^{-8}	[5]
CL-MOF-235/*β*-CD	1.0×10^{-8}-3.0×10^{-6}	1.0×10^{-8}	[7]
CL-MIL-53(Fe)	1.0×10^{-7}-1.0×10^{-5}	5.0×10^{-8}	[8]
CL-gold NPs	8.5×10^{-7}-1.0×10^{-4}	4.3×10^{-7}	[49]
CL-Co-Fe LDHs	5.0×10^{-8}-2.0×10^{-5}	2.0×10^{-8}	[50]
CL-carbon nitride quantum dots	5.0×10^{-7}-5.0×10^{-5}	1.0×10^{-7}	[51]
CL-GOD/GNPs/CNTs	2.25×10^{-6}-1.75×10^{-4}	1.0×10^{-6}	[52]
CL-CF-$CoFe_2O_4$ NPs	5.0×10^{-8}-1.0×10^{-5}	1.0×10^{-8}	[53]
CL-$CoFe_2O_4$ MNPs	1.0×10^{-7}-1.0×10^{-5}	2.4×10^{-8}	[54]
CL-WS_2NS and AgNCs	3.0×10^{-8}-2.0×10^{-5}	1.3×10^{-8}	[55]
CL-Hemin@HKUST-1	7.5×10^{-6}-7.5×10^{-4}	7.5×10^{-6}	[56]
CL-FeCo@NC-600	1.0×10^{-8}-1.0×10^{-5}	8.5×10^{-9}	This work